

The principle underlying antiaromaticity

Raphael J. F. Berger^{1*} and Alexandre Viel²

¹Department for Chemistry and Physics of Materials, University of Salzburg,
Jakob-Haringerstr 2a, A-5020 Salzburg, AUSTRIA

²8 Sente de la haie Saint-Marc, 78480 Verneuil sur Seine, FRANCE

*To whom correspondence should be addressed; E-mail: raphael.berger@sbg.ac.at.

Abstract

Aromaticity is one of the most widely used chemical concepts. Current definitions are purely phenomenological and relate symmetry, reactive stability and the occurrence of molecular diamagnetic response currents. The antithetical concept of antiaromaticity provides a connection between the contrary properties: structural instability or distortion out of higher symmetry, a small HOMO—LUMO gap, and paramagnetic response currents. We reveal the principle that is underlying antiaromaticity by showing an intimate and strict symmetry induced relation between these properties. This principle is mathematically rigorous and can be formulated like: *First order (and related) Jahn-Teller distorted molecules out of non-isometric point groups are prone to paramagnetic current susceptibility parallel to the main axis of symmetry.* We show by the exemplary cases of cyclobutadiene, cyclooctatetraene, pentalene and manganese trifluoride how this principle works and discuss this new perspective on antiaromaticity.

Aromaticity is one of the most widely used chemical concepts. It aims at an abstraction of different experimentally observed properties in a class of chemical compounds. These properties are typically a high structural or energetic stability, proneness to specific chemical reactions and susceptibility to induced diamagnetic currents when at the same time a theoretical description or also experimental evidence suggests a specific type of electronic structure. One often encounters this in the form of electron count rules, orbital occupation patterns or electronic resonance¹. A good overview about the state of research on aromaticity including references to a selection of current reviews is given in the introduction of ref.² While the connection of some of these

properties seems obvious, no concise connection between all in full generality could ever be established. Here we analyze the antithetical concept of *antiaromaticity* which was originally introduced by Breslow³ and find an intimate symmetry relation between its defining properties that so far seems to have escaped the general attention. Along the lines of the definition of antiaromaticity from the Gold Book of the International Union of Pure and Applied Chemistry (IUPAC)^{4,5} these are the three properties a) "... prone to reactions causing changes in their structural type, and display tendency to alternation of bond lengths and fluxional behavior ...", b) "... a small energy gap between their highest occupied and lowest unoccupied molecular orbitals ..." and c) "... an external magnetic field induces a paramagnetic electron current." A full quote of the definition is given in the Supplementary Information section. To show how these properties are related we use the following arguments

- Paramagnetic molecular response is determined by virtual electronic excitations of rotational symmetry, where the axis of rotation is parallel to the magnetic field.
- Ground state—excited state (or HOMO—LUMO) symmetries that give rise to virtual electronic excitations of rotational symmetry are arising from certain Jahn-Teller (JT) distortions out of specific molecular point group symmetries.
- These certain JT distortions are first order JT distortions (or closely related ones, which we later call *primoid* second order JT distortions) and happen out of point group symmetries that are non-isometric. That is from one of the point groups C_n , C_{nv} , C_{nh} , D_n , D_{nh} for $n > 2$, and D_{nd} and S_{2n} for $n > 1$.

A consequence of these arguments and our main result is

First order and primoid second order JT distorted molecules out of non-isometric point groups are prone to paramagnetic current susceptibility parallel to the main axis of symmetry.

We then advocate the view that this is the symmetry principle underlying antiaromaticity. After derivation of these results we discuss some exemplary cases and important implications of this new perspective on antiaromaticity for past and future research and a possible extension to the concept of aromaticity.

The occurrence of paramagnetic response currents is one of the three central defining properties of antiaromatic molecules. We start the results section with a derivation of a symmetry based "selection rule" for virtual electronic excitations determining paramagnetic response currents.

Results

Paramagnetic response currents

When a molecule is exposed to a magnetic field \mathbf{B} , that is in the simplest case static, homogeneous and weak, which we assume throughout this work, it interacts to first order via the total electronic angular momentum and total spin which correspond to permanent molecular magnetic moments. In case the expectation values of both are identical zero, *i.e.* closed shell singlet molecules, it only interacts to second order via its molecular magnetisability which is for bulk mater also called magnetic susceptibility. In the quasi-classic Bohr model of electrons circling around the nucleus such a field dependent magnetization corresponds to a superimposed precession motion of the orbiting electrons in the field \mathbf{B} . While a magnetization in this quasi classical picture must lead to an increase of the energy of the electronic system and hence is classified as diamagnetic response, in the quantum mechanical case the magnetic response in general can be partitioned into either diamagnetic or paramagnetic contributions. Such a paramagnetic magnetization has no quasi-classical counterpart, it however would correspond to a \mathbf{B} field dependent gain in angular momentum, leading to an energetic stabilization of the system. Also the partitioning into dia- and paramagnetic response contribution in general depends on the choice of the gauge, or in the particular case of a vector potential \mathbf{A} of the form $\mathbf{A}_d(\mathbf{r}) = (\mathbf{r} - \mathbf{d}) \times \mathbf{B}$ on the choice of the gauge origin \mathbf{d} . A natural choice for the gauge origin, however is the origin of reference \mathbf{r}_0 for the definition of the angular momentum (operator) $\mathbf{l} = (\mathbf{r} - \mathbf{r}_0) \times \mathbf{p}$, by the momentum (operator) \mathbf{p} , which serves also as centre of symmetry in case of non-trivial molecular symmetries and conveniently can be used as origin of the inner coordinate system of the molecule (then $\mathbf{r}_0 = \mathbf{0}$). According to McWeeny's perturbation theoretic formulation⁶ and orienting a unit strength magnetic field along the z axis: $\mathbf{B} = (0, 0, 1)^T = \mathbf{B}_z$, the paramagnetic part of the magnetically induced current density field $\mathbf{J}_p^{\mathbf{B}_z}(\mathbf{r})$ is obtained by

$$\mathbf{J}_p^{\mathbf{B}_z}(\mathbf{r}) = -\frac{2ne}{m_e} \Re \int d\mathbf{s}_1 d\mathbf{x}_2 \dots d\mathbf{x}_n \Psi^{\mathbf{B}_z*}(\mathbf{x}_1, \dots, \mathbf{x}_n) \mathbf{p} \Psi_0(\mathbf{x}_1, \dots, \mathbf{x}_n) \quad (1)$$

with the n the number of electrons, the electronic charge $-e$, the electron mass m_e , and the ground state wave function Ψ_0 that depends on spatial coordinates of the i -th electron \mathbf{r}_i and its spin coordinate \mathbf{s}_i which are combined to the space-spin coordinate \mathbf{x}_i and the (purely imaginary) first order magnetic response contribution to the wave function

$$\Psi^{\mathbf{B}_z}(\mathbf{x}_1, \dots, \mathbf{x}_n) = -\frac{e}{2m} \sum_{j>0} \Psi_j \frac{\langle \Psi_j | \mathbf{l}_z | \Psi_0 \rangle}{\varepsilon_j - \varepsilon_0}, \quad (2)$$

using \mathbf{l}_z for the z -component of the (total) angular momentum operator (alternatively an effective one-particle picture formulation can be easily obtained, resulting in an completely analogous expression for occupied-unoccupied orbital excitations). Thus the possibility of occurrence of a paramagnetic response contribution $\mathbf{J}_p^{\mathbf{B}_z}(\mathbf{r})$ is determined by the condition

$$\frac{|\langle \Psi_j | \mathbf{l}_z | \Psi_0 \rangle|}{\varepsilon_j - \varepsilon_0} > 0, \quad (3)$$

which in turn can be interpreted as a selection rule for $\mathbf{J}_p^{\mathbf{B}_z}(\mathbf{r})$ requiring the possibility of virtual excitations between Ψ_0 and Ψ_j of rotational symmetry with respect to an axis parallel to z , which is the direction of the magnetic field \mathbf{B}_z . The connection between paramagnetism and rotation to the best of our knowledge was pointed out for the first time by Steiner & Fowler⁷. According to the Wigner-Eckart theorem we can formulate the selection rule, that the decomposition of the direct (tensor) product of the irreducible representations (IRs, Γ) of the ground and excited states must contain the IR of the z -component of the angular momentum operator:

$$\Gamma_{\mathbf{l}_z} \subseteq \Gamma_{\Psi_j^*} \otimes \Gamma_{\Psi_0}. \quad (4)$$

The terms and hence total paramagnetic currents in general will be the stronger the larger the integrals $|\langle \Psi_j | \mathbf{l}_z | \Psi_0 \rangle|$ and the smaller the energy gaps $\varepsilon_j - \varepsilon_0$ between the engaged states are.

In this specific choice of gauge, that is a common gauge origin, one can introduce the terms dia- and paratropic⁸, which are referring to ring current contributions to the total current density vector field that are flowing either in classical direction or anti-classical direction around the gauge origin and with respect to the external magnetic field, thus giving rise to a dia- or paramagnetic induced magnetisation inside this ring current domain, respectively.

Representations of angular momentum components play now a central role in our considerations. In the following we will see that there is an intimate connection between tensor squares of two-dimensional IRs and representations of angular momentum components in certain point groups.

Angular momentum in squares of degenerate IRs

For here on we adopt the Mulliken conventions of A/a , and B/b for one-dimensional, E/e for two-dimensional, T/t for three-dimensional irreducible representations over \mathbb{R} , ρ for a general representation, Γ for an irreducible one and Γ_0 for the trivial (= totally symmetric) representation. Also in this whole work we consider only representations over \mathbb{R} .

Classifying the point groups by the dimensions of their IRs yields a partition into three sub-families that we call \mathcal{K}_{aaa} , \mathcal{K}_{ae} and \mathcal{K}_t . In informal chemical terminology point groups from \mathcal{K}_{aaa} are those which only have one-dimensional IRs (over \mathbb{R} , as used throughout), point groups from \mathcal{K}_{ae} are those which have two- but no higher dimensional IRs and point groups from \mathcal{K}_t have three- (or higher) dimensional IRs.

Table 1: Angular momentum and $E \otimes E$ representation tables for all point groups

(a) \mathcal{K}_{aaa} point groups

p.grp	C_1	C_s	C_2	C_i	C_{2v}	C_{2h}	D_2	D_{2h}
Γ_{1_z}	A	A'	A	A	A_2	A_g	B_1	B_{1g}

(b) \mathcal{K}_{ae} cyclic-based point groups

p.grp, $n \geq 1$	C_{2n+1}	C_{2n+2}	$C_{(2n+1)v}$	$C_{(2n+2)v}$	$C_{(2n+1)h}$	$C_{(2n+2)h}$	$S_{4n}^{(*)}$	S_{4n+2}
$\Gamma_e, i = 1 \dots n$	E_i	E_i	E_i	E_i	E'_i, E''_i	E_{ig}, E_{iu}	E_i	E_{ig}, E_{iu}
Γ_{1_z}	A		A_2		A'	A_g	A	A_g
$[\Gamma \otimes \Gamma]$	A		A_2		A'	A_g	A	A_g

(*) : i ranges from 1 to $2n - 1$

(c) \mathcal{K}_{ae} dihedral-based point groups

p.grp, $n \geq 1$	D_{2n+1}	D_{2n+2}	$D_{(2n)d}^{(*)}$	$D_{(2n+1)d}$	$D_{(2n+1)h}$	$D_{(2n+2)h}$
$\Gamma_e, i = 1 \dots n$	E_i	E_i	E_i	E_{ig}, E_{iu}	E'_i, E''_i	E_{ig}, E_{iu}
Γ_{1_z}	A_2		A_2	A_{2g}	A'_2	A_{2g}
$[\Gamma \otimes \Gamma]$	A_2		A_2	A_{2g}	A'_2	A_{2g}

(*) : i ranges from 1 to $2n - 1$

(d) \mathcal{K}_t type cubic point groups

p.grp	T		$T_d = O$			T_h				O_h					
Γ_l	T		T_1			T_g				T_{1g}					
Γ	E	T	E	T_1	T_2	E_g	T_g	E_u	T_u	E_g	T_{1g}	T_{2g}	E_u	T_{1u}	T_{2u}
$[\Gamma \otimes \Gamma]$	A	T	A_2	T_1	T_1	A_g	T_g	A_g	T_g	A_{2g}	T_{1g}	T_{1g}	A_{2g}	T_{1g}	T_{1g}

(e) \mathcal{K}_t type icosahedral groups

p.grp	I				
Γ_1	T_1				
Γ	T_1	T_2	G		H
$[\Gamma \otimes \Gamma]$	T_1	T_2	$T_1 \oplus T_2$		$T_1 \oplus T_2 \oplus G$

p.grp	I_h							
Γ_1	T_{1g}							
Γ	T_{1g}	T_{2g}	G_g		H_g		T_{1u}	T_{2u}
$[\Gamma \otimes \Gamma]$	T_{1g}	T_{2g}	$T_{1g} \oplus T_{2g}$		$T_{1g} \oplus T_{2g} \oplus G_g$		T_{1g}	T_{2g}

We now put our focus on the symmetry properties of the quantum mechanical total angular momentum operator \mathbf{l} and its z -component \mathbf{l}_z in the three point group families. A comparison with Table 1 shows that for all two-dimensional IRs E for all groups $G \in \mathcal{K}_{ae}$ the decomposition of the tensor square of E into irreducible representations always contains Γ_{1_z} , namely in its anti-symmetric part. In particular

$$E \otimes E = \Gamma_{1_z} \oplus \Gamma_0 \oplus \rho_q; \quad \dim(\Gamma_0) = \dim(\Gamma_{1_z}) = 1, \dim(\rho_q) = 2, \quad (5)$$

with

$$[E \otimes E] = \Gamma_{1_z} \quad (6)$$

holds, with $[M]$ denoting the anti-symmetric part of a tensor M (below and in the SI section $[M]$ is identified with the so called “alternating square” functor $Alt^2(M)$).

On the contrary, for groups from \mathcal{K}_t , $[E \otimes E]$ does not represent (any components) of \mathbf{l} (see Table 1). Rigorous definitions and reasoning, the relation between \mathbf{l} and the representation space $O(3)$ and further detailed outlines are given in the SI section.

So we see that in point groups from \mathcal{K}_{ae} there is an intimate connection between two-dimensional IRs and Γ_{1_z} . In the next section we consider branchings of two-dimensional electronic levels at a group theoretical level.

Distortions

Distorting a molecule from a higher to a lower symmetric structure leads to a restriction of the representations of molecular eigenstates to a subgroup H of G , which can change the shape of its irreducible decomposition. This is usually called ‘descent in symmetry’ in chemistry, the mathematical discipline concerned with this is ‘branching representation theory’.

Consider a point group $\mathcal{H} \subset \mathcal{G}$, and a two dimensional representation E of \mathcal{G} . If the restriction of E to \mathcal{H} ($= E|_{\mathcal{H}}$) branches into a direct sum of two one-dimensional representations of \mathcal{H} ,

$$E|_{\mathcal{H}} = A_\alpha \oplus A_\beta \quad (7)$$

then

$$[E \otimes E]|_{\mathcal{H}} = [E|_{\mathcal{H}} \otimes E|_{\mathcal{H}}] = A_\alpha \otimes A_\beta \quad (8)$$

as is lined out in the SI section in subsection S1. If E was the representation of the point group \mathcal{G} on the (x, y) -plane, then

$$\Gamma_{\hat{l}_z}|_{\mathcal{H}} = [E \otimes E]|_{\mathcal{H}} = A_\alpha \otimes A_\beta. \quad (9)$$

The angular momentum representation of \mathcal{H} on the rotations around the z -axis is the tensor product of the two representations A_α, A_β .

This implies that if an E -type IR in a non-isometric point group is restricted to a subgroup such that it splits into two non-degenerate hence one-dimensional IRs, then the direct product of these two one-dimensional representations is exactly the representation of the z-component of the angular momentum operator (in the subgroup). This is an essential result.

In particular the Jahn-Teller (JT) distortions to be discussed in the next section can trivially be described as a descent in symmetry, such that all considerations from above are valid for JT distortions.

'Primoid' second order JT systems

We adopt in the following a simplistic view on the Jahn-Teller-Effect based on the original idea from Landau and Teller where distortions were considered in the form of small perturbations and based on a specific situation of electronic degeneracy. As a starting point for a deeper understanding and a contemporary view on the JT-effect we refer the reader to I. B. Bersuker's introductory text "Recent Developments in the Jahn-Teller Effect theory"⁹. We are focusing only on the basic integrals occurring in the perturbation expansion¹⁰ of the molecular energy with respect to a deviation (or distortion) Q from the minimum geometry on the adiabatic potential energy surface. In general Q may be regarded as some symmetry adapted local nuclear distortion coordinate, like a vibrational normal modes. In that sense the occurrence of a first order JT distortion is determined by the size of the first order coefficients in Q :

$$\langle \Psi_0 | \frac{d\hat{H}}{dQ} | \Psi_0 \rangle \quad (10)$$

with the ground state wave function Ψ_0 , while second order JT distortions are controlled by the negative components of the second order coefficients¹⁰

$$\sum_{i>0} \frac{\left| \langle \Psi_0 | \frac{\partial \hat{H}}{\partial Q} | \Psi_i \rangle \right|^2}{\varepsilon_0^0 - \varepsilon_i^0} \quad (11)$$

with the virtual state wave functions Ψ_i , and the corresponding unperturbed state energies ε_j^0 (for $j = 0, i$).

Let us consider now a one electron (for simplicity) molecule in a twofold degenerate, E type, one-electron state ψ_0 , then the JTT implies that for a non-linear point group symmetry G a non-totally symmetric distortion mode Q exists such that according to expression 10 we have $\Gamma_Q \subseteq \Gamma_{\psi_0}^* \otimes \Gamma_{\psi_0}$.

When we now interpret this one-electron E state as a spatial orbital from which we can built two-electron configuration state functions from symmetry adapted linear combinations of Slater

determinants of these (spin)orbitals, we arrive at various possible combinations of ground and virtual state (Ψ_0 and Ψ_i) symmetries: $\Gamma_{\Psi_0}, \Gamma_{\Psi_i} \subset \Gamma_{\psi_0} \otimes \Gamma_{\psi_0} = \Gamma_0 \oplus Alt^2(E) \oplus \rho_q$ (with eq. 5). From those one can choose $\Gamma_{\Psi_0} = \Gamma_0$ and $\Gamma_{\Psi_i} = \Gamma_Q$, yielding, as the Wigner-Eckart theorem applied to expression 11 suggests $\Gamma_Q \subseteq \Gamma_{\psi_0}^* \otimes \Gamma_{\psi_i} = \Gamma_0 \otimes \Gamma_Q = \Gamma_Q$, such that a second order JT distortion by the mode Q is possible. Such a choice we call “**primoid** second order JT system”. In the practice of quantum chemical calculations, primoid second order JT systems reveal their nature in the orbital space from which their state functions can be constructed. This is demonstrated in the degeneracy and branching of orbital energies like in C_4H_4 (see below and Fig. 1).

Also, by this two-electron wave function construction, from an one-electron wave function, both Ψ_0 and the virtual state Ψ_i can only be in the decomposition of $E \otimes E$, which together with the restriction to cases where JT causes only small structural perturbations can warrant that the energy denominator in expression 11 is not too large.

For a counter example of a *non-primoid* second order JT case, consider Si_4F_4 in the abelian D_{2h} symmetry¹¹ which distorts via a B_{1g} mode to C_{2h} , or similarly $Si_2Ge_2F_4$ which distorts from D_{2h} via C_{2h} to C_s . In general, all cases of second order Jahn-Teller distortion which are of a reference (or highest possible) point group symmetry that possesses no degenerate IRs over \mathbb{R} , are non-primoid second order Jahn-Teller cases.

JT and paramagnetism in point groups from \mathcal{K}_{ae}

All point groups G in the family \mathcal{K}_{ae} (see Table 1) are represented by at least one two-dimensional IR over \mathbb{R} , say E and in these point groups $Alt^2(E)$ represents for all E the z -component of the quantum mechanical angular momentum operator I_z . Now molecular systems in electronic states represented by E are due to their degeneracy prone to a first order JT distortion. If such a distortion to a subgroup H of G occurs then E branches into two one-dimensional representations, say A_α and A_β . The corresponding lower lying electronic state say A_α eventually will become the ground state (or a SOMO or HOMO orbital in the effective one-particle picture) while the higher lying state A_β will become some virtual state (or a UMO or possibly the LUMO depending on the size of the distortion). Then and especially if the distortion is not too large, such that the energy difference between occupied and virtual states will not become too large, the system becomes by virtue of the symmetry selection rule for paratropic currents (eqns. 1 and 3) strongly susceptible to induced paratropic currents (since according to eq. 9 $A_\alpha \otimes A_\beta = \Gamma_{I_z}$). In this way we see that all first order JT cases arising from point groups G in the family \mathcal{K}_{ae} , that is all non-isometric first order JT cases, are inherently prone to paramagnetism.

Since this result is based on group theoretical considerations it can be seen as a completely

general symmetry property that combines structure and magnetic response. Similar like *e.g.* the dipole transition rule which gives a general symmetry property of the molecular response with respect to any dipole fields. Like such spectroscopic selection rules, the predictivity is of course limited by the fact that we deal merely with symmetry rules which are completely independent of the peculiar quantitative electronic properties of a molecule under investigation. But also similar to these selection rules the principle might serve as a basis for the understanding of the phenomenon of antiaromaticity in a very general sense.

It is very important to note that these considerations are not restricted to the first order JT effect since this is bound to open shell systems, and the most important examples for antiaromaticity like 1,3-cyclobutadiene are closed shell cases. From the definition of the *primoid* second order JT case it follows immediately that there is the very same connection between symmetry and paratropic response currents. One example is 1,3-cyclobutadiene, that goes back to states derived from a doubly occupied doubly degenerate orbital.

We now can formulate the main result of this work, as is announced in the introduction:

First order and primoid second order JT distorted molecules out of non-isometric point groups are prone to paramagnetic current susceptibility parallel to the main axis of symmetry.

Assuming small distortions, it is clear that these cases match the complete IUPAC definition of antiaromaticity (see Introduction and SI) such that a strict connection between the defining properties is given. Since to the best of our knowledge there exists no undoubted example for an antiaromatic molecule that does not belong to this class, we suggest that this is the symmetry principle underlying antiaromaticity.

In the following we will discuss four representative examples for molecules, each of them reflecting a slightly different situation in hindsight to its antiaromatic character.

Examples

C_4H_4

1,3-Cyclobutadiene (C_4H_4) is such a prominent example for antiaromaticity that it is mentioned in the IUPAC definition (see ref.^{4,5} and the SI for a full quote). Details on its symmetry, electronic states and the nature of the Jahn-Teller distortion have been worked out by Nakamura & co-workers¹² in the framework of a MCSCF study. It is a case where for the full D_{4h} symmetry we have double occupation of the doubly degenerate e_g orbitals (e_g^2), which results in purely non-degenerate electronic states, the first four of which are in energetically ascending order $^1B_{1g}, ^3A_{2g}, ^1A_{1g}, ^1B_{2g}$. Hence, this is a prototypical example for a primoid second order Jahn-Teller case.

Formally removing one electron yields the $[\text{C}_4\text{H}_4]^+$ cation and a 2E_g ground state. To check the possibility of a non-zero integral term 10, thus the possibility of existence of a distortional mode Q leading to an energetic stabilization, which is a condition for a first order JT effect, we need to decompose $E_g \otimes E_g$ into a direct sum of IRs. This yields

$$E_g \otimes E_g = A_{1g} \oplus [A_{2g}] \oplus B_{1g} \oplus B_{2g} \quad (12)$$

Permissible distortional mode symmetries (as must be checked separately) here are either B_{1g} or B_{2g} , these are related by a 45° rotation around z , and give rise either to a rhombic or a rectangular D_{2h} symmetric structure, respectively. Quantum chemical calculations show that in this case the rhombic structure is preferred¹² and leads to a splitting of the degenerate e_g orbitals into two non-degenerate b_{2u} and b_{3u} orbitals.

Since D_{4h} is a non-isometric point group (case \mathcal{K}_{ae}) and E_g is a degenerate level we know according to eq. 5 that $E_g \otimes E_g$ contains the IR for the z -component of the angular momentum Γ_{1_z} , which in D_{4h} is A_{2g} . Moreover from eq. S3 follows that this is $\Gamma_{1_z} = \text{Alt}^2(E_g) = [E_g \otimes E_g] = A_{2g}$. According to eq. 9 in the new group D_{2h} the IR for 1_z is contained in the direct product of the two branches of E_u . That this is indeed the case shows a quick check: in D_{2h} we have $B_{2u} \otimes B_{3u} = B_{1g}$, which is identical to Γ_{1_z} in this group.

As we have identified C_4H_4 by its orbital structure as a (potential) primoid second order JT case by recursion to the hypothetical $[\text{C}_4\text{H}_4]^+$ case, we could easily identify the possible symmetries of the Q mode that could be operational in a second order JT effect. Note that since this a (primoid) second order JT distortion no electronic state degeneracy is involved but only a coupling between the ${}^1B_{1g}$ ground state and an ${}^1A_{1g}$ excited state takes place which is moderated by the B_{1g} type distortion. The degeneracy and branching only is reflected in the underlying orbital structure which leads to the classification as a *primoid* second order JT system. And in addition by the arguments from above on the angular momentum representation we know that in the “real” n -electron state case with a $(e_g)^2$ occupation there will be occupied-to-virtual transitions of Γ_{1_z} a symmetry species available in the accordingly distorted molecule.

We can verify this as well: Eq. 12 shows all permissible two electron states from the $(e_g)^2$ occupation. As a matter of fact the ground state turns out to be of a ${}^1B_{1g}$ symmetry species and out of the virtual states given by the remaining three terms of eq. 12 again only a virtual transition to the ${}^1A_{1g}$ state is of a symmetry species that is in accordance with a permissible distortional coordinate Q (see $[\text{C}_4\text{H}_4]^+$ case), that is

$$B_{1g} \otimes A_{1g} = B_{1g}. \quad (13)$$

So both models predict of course the same possible symmetries of distortion Q out of D_{4h} into D_{2h} . To find the by virtue of the “primoid” argument predicted virtual transition of Γ_{1_z} symmetry species we have to restrict all terms on the right side of eq. 12 to the subgroup D_{2h} .

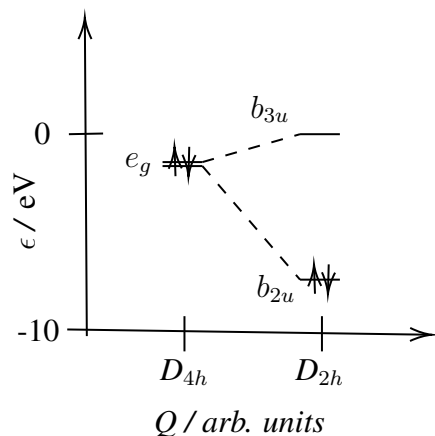


Figure 1: Frontier orbital energies ϵ for the ground state saddle point (D_{4h}) or minimum structure (D_{2h}) calculated at the generalized valence bond - perfect pairing (GVB(PP)/TZVPP) level of theory for cyclooctatetraene (C_8H_8). Orbital energy splitting upon distortion Q from D_{4h} to the D_{2h} minimum is indicated by the dashed lines. The distortion from $D_{4h} \rightarrow D_{2h}$ is a *primoid* second order Jahn-Teller (JT) distortion via a B_{1g} mode. The corresponding electronic levels are shown in Fig. S2 in the SI. Note that the electronic levels are *not degenerate* (second order JT system), but the underlying orbital structure that is depicted here shows degeneracy and branching (*primoid* second order JT system). The direct products $E_g \otimes E_g$ and $B_{2u} \otimes B_{3u}$, the latter corresponding to the paramagnetic virtual excitation, contain or are the IR for the z -component of the angular momentum operator. The molecule in the D_{4h} saddle point configuration shows a much stronger paramagnetic response than the D_{2h} minimum structure (compare Fig. 3) but both are classified as antiaromatic.

This gives

$$(A_{1g} \oplus A_{2g} \oplus B_{1g} \oplus B_{2g})|_{D_{2h}} = A_g \oplus B_{1g} \oplus A_g \oplus B_{1g} \quad (14)$$

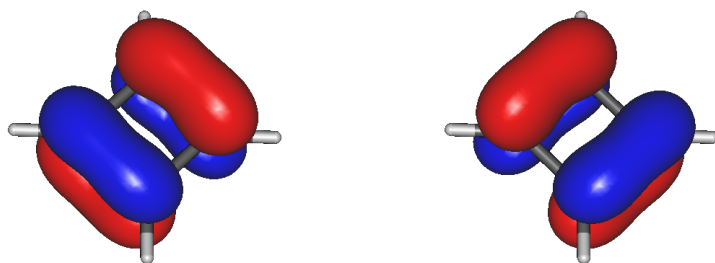
Since thus the ground state “branches” from B_{1g} to A_g , for example a virtual transition $A_g \rightarrow B_{1g}$ is available which corresponds obviously to a B_{1g} symmetry species and, that as we have used already above, is identical to Γ_{1z} in D_{2h} .

So we have shown how the argument of prediction of virtual transitions of Γ_{1z} symmetry, that is paramagnetic response, for the *primoid* second order JT case C_4H_4 (out of non-isometric point groups) works. Calculations show (see SI for details) that we can expect a double bond localization, or at least a splitting of C-C distances from 1.426 Å (D_{4h}) to 1.552 and 1.324 Å. The weight of the second configuration is about 4% at the D_{2h} minimum structure, thus it is safe to use a single reference method for calculation of the magnetically induced ring currents (see SI for details). The integral of the total global current susceptibility amounts to -22.4 nA/T paratropic total current at HF/VTZ level of theory.

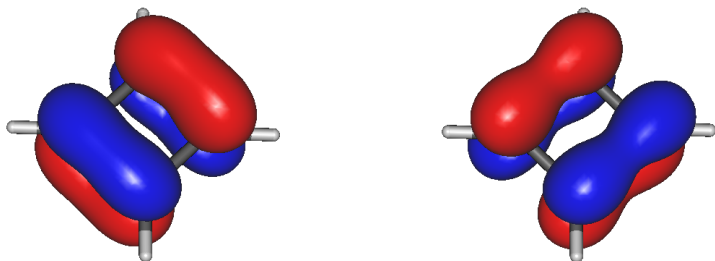
For the aromatic benzene we find diamagnetic current contributions of about +20 nA/T. One

might say C_4H_4 is as paramagnetic as benzene is diamagnetic (but one should note that there are paramagnetic contributions to the benzene currents as well and these are of a size of about -9 nA/T)¹³.

C_4H_4 is the classical example for antiaromaticity, in agreement with that we find that its ground state geometry is derived from a primoid second order Jahn-Teller distortion out of a point group of the family \mathcal{K}_{ae} , it has a small HOMO-LUMO gap and thus as a consequence of the latter two arguments shows a strong paramagnetic response with respect to a magnetic field B parallel to the original C_4 axis.



(a) Highest occupied molecular orbital (HOMO) in the D_{4h} saddle point structure. The two-fold degenerate orbital is represented by the e_g IR.



(b) HOMO (left) and lowest unoccupied molecular orbital (LUMO, right) in the D_{2h} minimum structure. The HOMO is represented by b_{2u} , the LUMO by the b_{3u} IR.

Figure 2: Frontier orbitals of the electronic ground state in C_4H_4 at different symmetries, calculated at the GVB(PP)/TZVPP level of theory, displayed as isosurfaces at densities of 0.066.

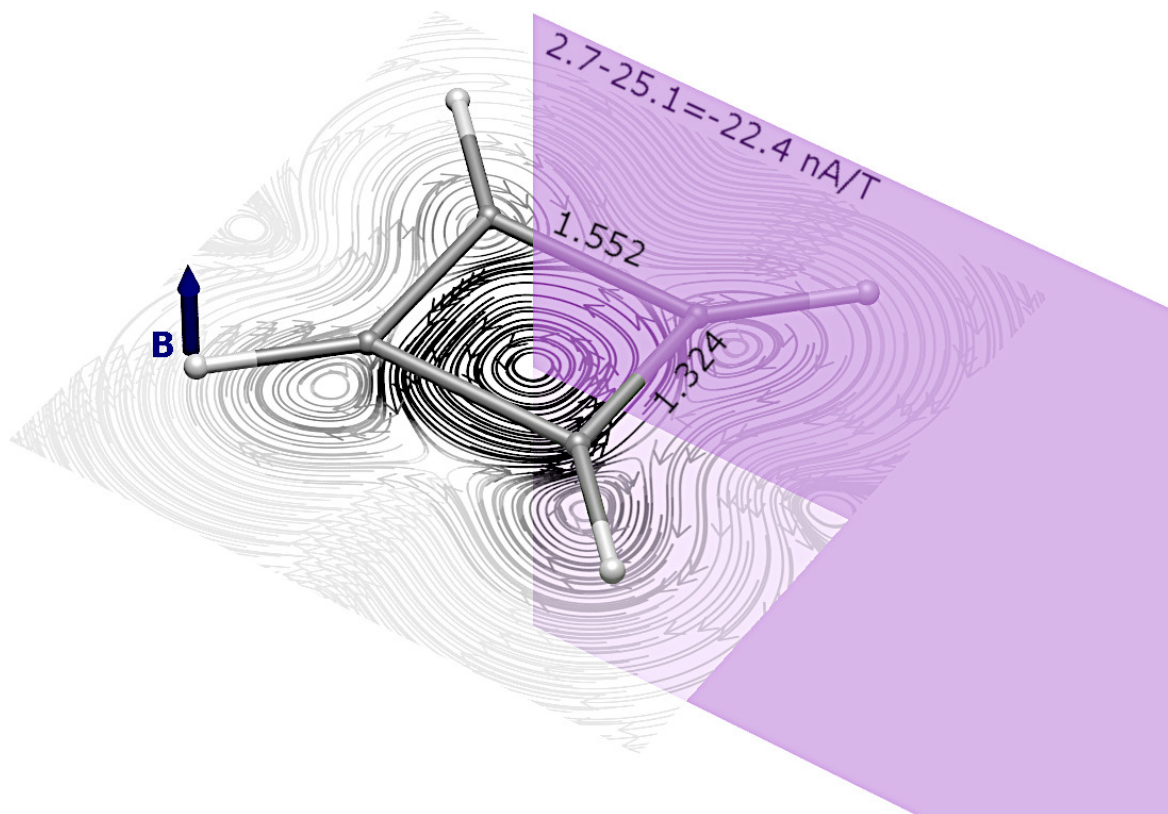


Figure 3: D_{2h} electronic ground state, minimum structure (distances given in units of Å) of C_4H_4 , and stream line plot of magnetically induced (field direction indicated by the blue arrow) currents at a plane 0.5 Å, below the molecular plane. Integration of currents flowing through the purple surface yields a global molecular ring current of -22.4 nA/T (paratropic).

C_8H_8

Another example from the compound class of the n -annulenes is cyclooctatetraene (C_8H_8) which is similar to C_4H_4 in that it represents also a primoid second order JT case, but as we will see shows some quantitative difference in its paramagnetic response.

The idealized D_{8h} symmetry is not observed as a ground state minimum¹⁴ due to a primoid second order JT distortion (e_u^2 case). Also here we observe a B_{1g} distortion to a D_{4h} structure, which turns out to be no minimum structure either as it undergoes another second order JT distortion along a B_{1u} mode to a D_{2d} symmetric minimum structure. As the first distortion is

of primoid type we know that in D_{4h} , the IR Γ_{1_z} will be the tensor product of the branches of the e_u orbitals. As these are b_{1u} and b_{2u} and $b_{1u} \otimes b_{2u} = a_{2g}$ and $\Gamma_{1_z} = a_{2g}$ in D_{4h} we find our symmetry rule confirmed. Since C_8H_8 undergoes another second order JT distortion into D_{2d} we still find

$$\begin{aligned}(B_{1u} \otimes B_{2u})|_{D_{2d}} &= A_{2g}|_{D_{2d}} \\ B_{1u}|_{D_{2d}} \otimes B_{2u}|_{D_{2d}} &= A_2 \\ A_1 \otimes A_2 &= A_2\end{aligned}$$

In agreement with this A_2 represents Γ_{1_z} in D_{2d} , hence the prediction that the frontier orbital symmetries that were branching out of e_u in this sequence of primoid and non-primoid second order JT distortions relate to each other in Γ_{1_z} manner is confirmed (again note that the electronic levels themselves are not degenerate and branch but rather couple by the distortion, see also Fig. 4). In addition paramagnetic response for the D_{2d} minimum of C_8H_8 is predicted, since we started from a non-isometric point group symmetry.

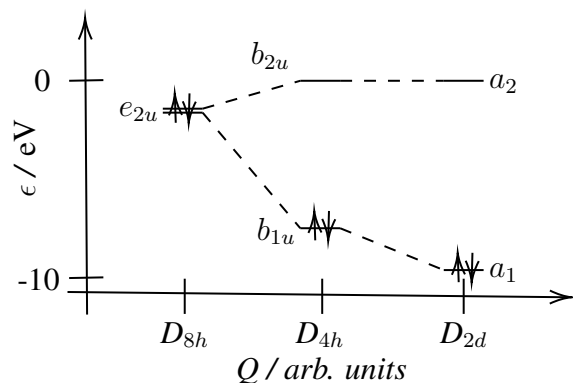
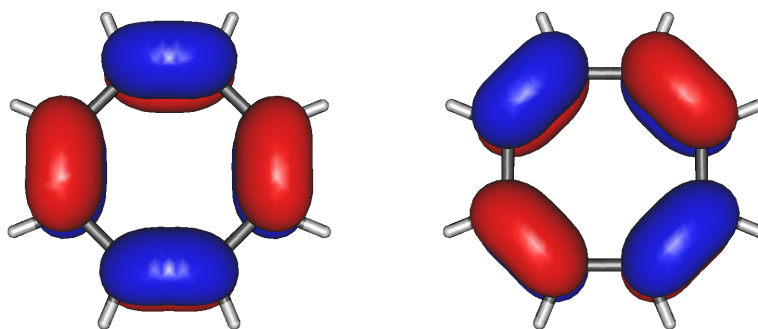
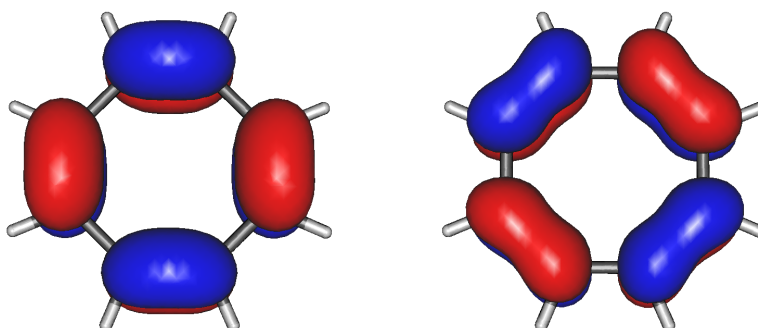


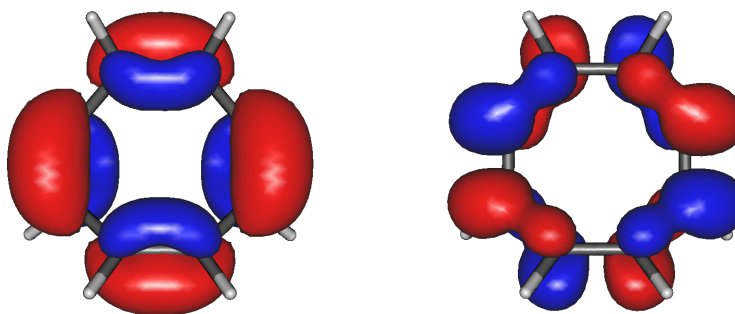
Figure 4: Frontier orbital energies ε for the ground state saddle point (D_{8h} of second order, D_{4h} of first order) or minimum structures (D_{2d}) calculated at the generalized valence bond - perfect pairing (GVB(PP)) level of theory for cyclooctatetraene (C_8H_8). Orbital energy splitting upon distortion Q from D_{8h} via D_{4h} to the D_{2d} minimum is indicated by the dashed lines. The first distortion $D_{8h} \rightarrow D_{4h}$ is a *primoid* second order Jahn-Teller (JT) distortion via a B_{1g} mode, the second one is a non-primoid JT distortion via a B_{1u} mode. Again, like in C_4H_4 the electronic ground state is non-degenerate (second order JT) but the underlying orbital levels show degeneracy and branching (primoid second order JT system). All three direct products $E_{2u} \otimes E_{2u}$, $B_{1u} \otimes B_{2u}$, and $A_1 \otimes A_2$, the latter two corresponding to the paramagnetic virtual excitation, contain or are identical to the IR for the z -component of the angular momentum operator. Virtual excitations represented by the terms given in expression 11 are not only decreasing by virtue of the increasing energy denominator but also due to the decreasing overlap integral in the numerator. Thus the molecule in the D_{4h} saddle point configuration shows a much stronger paramagnetic response than the D_{2d} minimum structure (compare Fig. 6).



(a) Highest occupied molecular orbital (HOMO) in the D_{8h} double saddle point structure. The two-fold degenerate orbital is represented by the e_{2u} IR.



(b) HOMO (left) and lowest unoccupied molecular orbital (LUMO, right) in the D_{4h} double saddle point structure. The HOMO is represented by b_{1u} , the LUMO by the b_{2u} IR.



(c) HOMO (a_1 , left) and LUMO (a_2 , right) in the D_{2d} minimum structure.

Figure 5: Frontier orbitals of C_8H_8 at different geometries, calculated at the GVB(PP)/TZVPP level of theory, displayed as isosurfaces at densities of 0.05.

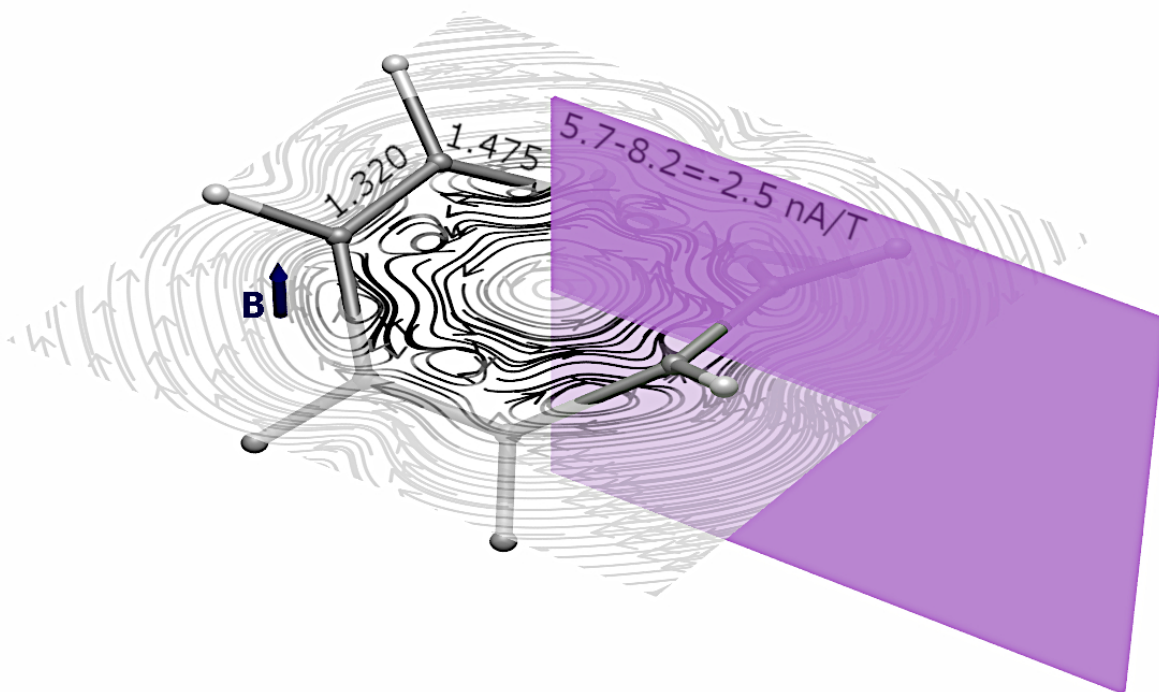


Figure 6: D_{2d} electronic ground state, minimum structure (distances given in units of Å) of C_8H_8 , and stream line plot of magnetically induced (field direction indicated by the blue arrow) currents in the average molecular plane (x, y -plane). Integration of currents flowing through the purple surface yields a global molecular ring current of -2.5 nA/T (purely paratropic contribution), which is comparably weak, thus the D_{2d} electronic ground state minimum structure of C_8H_8 is classified as weakly antiaromatic or non-aromatic.

In contrast to the markedly paramagnetic nature of the magnetic response of the ground state minimum of C_4H_4 (-21 nA/T) for C_8H_8 we find barely -2.5 nA/T total induced current. However, the paratropic contribution amounts to -8.2 nA/T, thus we again see the rule confirmed that first and primoid second order JT distortions lead to systems with paramagnetic response. In this case however the total paramagnetic response is too weak to assign the predicate “antiaromatic” to this molecule. One reason is that the *second* second order JT distortion (which for itself is not of primoid type since the degeneracy of the frontier orbital has already been lifted to b_{1u} and b_{2u}) causes a further increase of the HOMO-LUMO energy gap to 9.7 eV at GVB(PP) level of theory, thus diminishing the magnetic response accordingly. For comparison the value for C_4H_4 at the same level of theory (GVB(PP)) is 7.2 eV.

The General $4n$ π annulene and double bond localization (bond length alternation)

In antiaromatic n -annulenes ($C_{4n}H_{4n}$) in the idealized $D_{(4n)h}$ symmetry, double bond localisation can be easily understood as a second order (primoid) JT effect. The saddle point in these cases would have a double occupied e_{nu} or e_{ng} orbital, for even n or for odd n , respectively, thus an $(e_{nu})^2$ or $(e_{ng})^2$ configuration, respectively, that can distort via a b_{1g} mode to $D_{(2n)h}$ symmetry, leading to a branching of e_{nu} to b_{1u} and b_{2u} for even n and similarly with *gerade* symmetry species g for odd n , which would correspond in analogy to the above discussed C_8H_8 to a double bond localization in the first instance.

An introductory discussion of the view of double bond localisation in ring systems as a JT distortion as well as its relation to the Peierls distortion in polyethin is given in ref. ¹⁵.

MnF₃

Manganese trifluoride is a prime example for a first order Jahn-Teller effect which would give in D_{3h} (a non-isometric point group) an E' ground state. In fact the lowest energy species is in the 5B_1 electronic ground state and has a planar C_{2v} symmetric structure which was predicted theoretically and confirmed by gas-phase electron-diffraction¹⁶. Magnetic response calculations indeed show magnetically induced paratropic currents around the central manganese atom as well as locally around the fluorine atoms (see Figures 7 and 8).

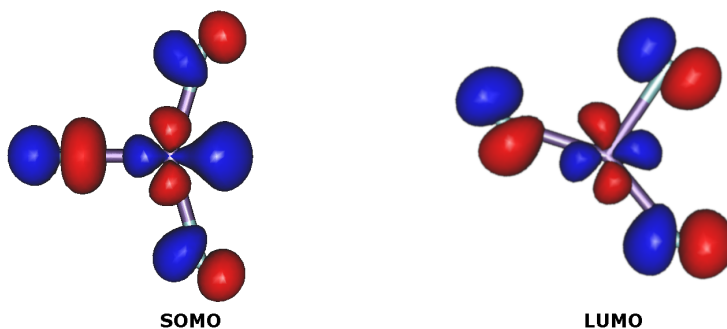


Figure 7: The 5B_1 electronic ground state structure of MnF_3 with C_{2v} symmetry and the b_1 α -HOMO and a_1 α -LUMO. The LUMO is displayed for a rotated molecule, the angle of rotation is about -120° . The rotational relation between the orbitals is already noticeable with bare eye.

Unlike in the previous two examples the induced paramagnetism is hidden to some extent, since experimentally the permanent magnetic moment resulting from spin dominates the magnetic properties and for the other since in this case the paramagnetic currents are atom-centered which hampers the computational analysis of the current densities due to interference with other atomic current contributions. In addition though, MnF_3 can be observed in the gas-phase¹⁶, in

condensed matter the coordinatively unsaturated threefold coordinated Mn^{3+} cation under normal conditions is not observable.

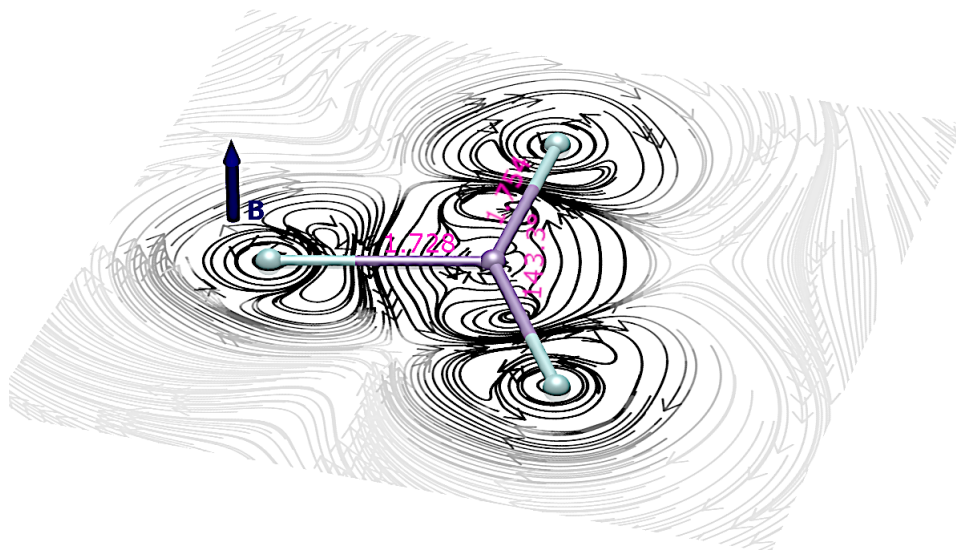
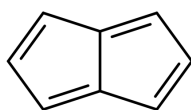


Figure 8: The 5B_1 electronic ground state structure of MnF_3 with C_{2v} symmetry and a streamline plot of the magnetically induced currents in the molecular plane (\mathbf{B} field is set perpendicular to the molecular plane). A paratropic current vortex (counterclockwise) around the Mn atom is found.

Pentalene

An interesting case that at first sight seems to be an outlier of our antiaromaticity symmetry rule is pentalene (see below for a molecular formula). Pentalene is a well-known case of antiaromaticity and its magnetisability was recently studied computationally¹⁷. Its apparent JT idealized symmetry would be D_{2h} (with HOMO a_u and LUMO b_{1u}) while its computationally predicted and experimentally confirmed minimum structure is C_{2h} (HOMO: a_u , LUMO a_u). However, D_{2h} is clearly a class \mathcal{K}_{aaa} point group, thus the observed $D_{2h} \rightarrow C_{2h}$ distortion cannot be interpreted as a primoid second order JT type distortion (as outlined in section), nevertheless we observe strong paramagnetic response which is dominated by the HOMO-LUMO virtual excitation and a distortion that is in agreement with a double-bond localisation. In essence the crucial argument in this case is that we have to deal with a ring system containing a set of conjugated double bonds on its perimeter. Thus a natural way of interpretation would be to classify pentalene as a perturbed eight membered ring, that derives from an idealized but

perturbed D_{8h} point group symmetry, with the perturbation being the additional transannular C-C bond. In this way the fact that the direct products of the HOMO-LUMO IRs are identical to the IR of I_z is mostly easily seen from the branching of D_{8h} 's E_{2u} into the A_u and B_{1u} IRs.



pentalene

Therefore pentalene cannot directly by using our symmetry rule be classified as an antiaromatic compound.

Chemical interpretation of dia- and paratropic response currents

Equation 2 means that a magnetic field probes the accessibility of virtual states that ideally differ from the ground state only by a rotational orientation of the wave function in space and thus are spatially very closely related. In case a molecule responds with a strong paratropic current density this can mean that there is a situation of close to degeneracy resembling the spatial symmetry of an atomic open subshell. The optimal symmetry/energy relation in question of eq. 2 in this way can be interpreted as the analog to an atomic open subshell case for a general molecular system, and the magnetic response is a concise probe for that. In addition one also yields information on the direction of the symmetry relation from the direction of the field \mathbf{B} .

The type of degeneracy that is probed by the magnetic field is not the only possible type. Other types of (near) degeneracy include ones derived from what is sometimes called “accidental” degeneracy where there is no obvious (close-to-)symmetry relation in $O(3)$ between occupied and empty levels and hence no contribution to paramagnetic response from these.

In contrast the antithetical concept of aromaticity is characterized by induced diamagnetic currents. In the common gauge origin approach, diamagnetic currents to first order are determined by the ground eigenstate Ψ_0 of the \mathbf{B} field free system and correspond to a precession motion of the electrons in the magnetic field that increases the average expected angular momentum $\langle \Psi | \hat{I}_z | \Psi \rangle$, (for Ψ the wave function in the magnetic field) which will lead in general if the ring current extends over a sufficiently large domain covering sufficiently much of the total electron density in the molecule to an increase in total energy.

An alternative way is to describe diamagnetic response via the “Continuous Transformation of the Origin of the Current Density” (CTOCD-DZ) approach that was introduced to theoretical

chemistry by Keith & Bader in 1992¹⁸ that allows in particular within to Fowler & Steiner’s ipsocentric *ansatz*⁷ to express the full magnetic response, completely in terms of occupied to virtual state (or orbital) transitions.

In this model the diamagnetic currents are determined by virtual transitions of dipole symmetry, namely dipole transition moments perpendicular to the external field \mathbf{B} . That means that for example sigma bonds that leave pairs of σ and σ^* type occupied and virtual orbitals, where the bond direction is perpendicular to the external field, contribute to the diamagnetic response. A simple example would be a bonding orbital that has some anti-bonding counterpart with a nodal plane parallel to \mathbf{B} .

In that way an electronic structure that contains covalent or systems of delocalized covalent bonds (and naturally the corresponding anti-bonding orbitals unoccupied) is diamagnetic. So we can summarize that a strong diamagnetic response current can be a consequence of (full) occupation of bonding orbitals and empty anti-bonding orbitals, which differ from bonding orbitals by additional nodal planes parallel to \mathbf{B} . Whereas paramagnetic response can indicate incompletely occupied molecular shells which are similar up to a rotation around an axis parallel to \mathbf{B} . This in effect leads to a distinctly different picture of antiaromaticity as it was originally envisaged by Breslow as he for instance noted “Thus antiaromaticity is a particular aspect of anti-bonding, just as aromaticity is a particular aspect of bonding”³, which is according to our analyses not the case since its not the occupation of anti-bonding orbitals that lead to the characteristic paramagnetic response currents, nor would it lead to a peculiar small HOMO-LUMO energy gap in general, or be connected with structural distortions.

At quick glance it might be surprising that antiaromaticity has often been observed or at least proposed for organic ring systems and related species like polycyclic molecules. In contrast antiaromaticity is rarely mentioned in the context of inorganic coordination compounds and metal clusters. On the bases of our findings this is easily explained, because the vast majority of organic ring systems and related compounds can be deduced from the particular point groups \mathcal{K}_{ae} , that is non-isometric point groups with degenerate real irreducible representations. In exactly this symmetry family we have the strict relation between JT distortion and paramagnetic response. While the majority of 3D-cluster systems or coordination compounds are derived from isometric point groups where this strict correspondence does not exist. In addition coordination compounds are of course metal-centered and at least experimentally the induced paramagnetism there is often masked by permanent magnetic moments centered at the metal atoms.

The here introduced analyses might serve as a basis for a deeper understanding of antiaromaticity, but despite its principle significance, antiaromaticity is not a widely spread chemical phenomenon (for obvious reasons, since it is not only connected with structural instability but also instability in the sense of high reactivity by virtue of the small energy gap between oc-

cupied and virtual states). At this stage one might speculate if there is some consistent way to define aromaticity by the absence of paramagnetism alone, an idea going back to Bilde & Hansen¹⁹. In that way the presence or absence of rotationally accessible virtual states and their intimate connection with structural distortions could eventually be the only decisive criteria for presence or absence of aromaticity or antiaromaticity.

An extension of these considerations we are currently working on is the analysis of the symmetry rules of magnetic response and JT distortion in the fully relativistic domain including spin-orbit coupling.

Conclusion

We have shown by symmetry considerations how Jahn-Teller distortion and paramagnetic response are intimately related in the family of point groups comprised of C_n , C_{nv} , C_{nh} , D_n , D_{nh} , for $n > 2$ and S_{2n} and D_{nd} for $n > 1$. We suggest that this connection is the underlying symmetry principle of antiaromaticity, since the latter is defined by the central properties of a small HOMO-LUMO gap, proneness to structural distortion or instability and magnetically induced paramagnetic ring currents. We also saw that electronic structure related to covalent or delocalized covalent bonding or filled atomic subshells followed by empty subshells is related to diamagnetic response while electronic situations resembling open atomic subshells are related to paramagnetic response. The sparsity of examples may not only go back to the fact that antiaromaticity is related to low energetic stability but also due the paradox between distortion and paramagnetism that is hidden under its definition and that we have revealed in this work.

References

- [1] Solà, M. Connecting and combining rules of aromaticity. Towards a unified theory of aromaticity. *WIREs, Comp. Mol. Sci.* (2018).
- [2] Janda, T. & Foroutan-Nejad, C. Why is benzene unique? Screening magnetic properties of C_6H_6 isomers. *Chem. Phys. Chem.* **19**, 2357–2363 (2018).
- [3] Breslow, R. Antiaromaticity. *Acc. Chem. Res.* **6**, 393–398 (1973).
- [4] International Union of Pure and Applied Chemistry, IUPAC Compendium of Chemical Terminology – The Gold Book (2006).
- [5] Minkin, V. I. Glossary of terms used in theoretical organic chemistry — Pure and Applied Chemistry. *Pure Appl. Chem.* **71**, 1919 – 1981 (2009).
- [6] Lazzeretti, P. Ring currents. *Prog. Nuc. Mag. Res. Spec.* **36**, 1 – 88 (2000).

- [7] Steiner, E. & Fowler, P. W. Four- and two-electron rules for diatropic and paratropic ring currents in monocyclic systems. *Chem. Commun.* 2220–2221 (2001).
- [8] Sulzer, D., Olejniczak, M., Bast, R. & Saue, T. 4-component relativistic magnetically induced current density using London atomic orbitals. *Phys. Chem. Chem. Phys.* **13**, 20682–20689 (2011).
- [9] Bersuker, I. B. Recent developments in the Jahn–Teller effect theory. In Köppel, H., Yarkony, D. & Barentzen, H. (eds.) *The Jahn-Teller Effect*, vol. 97 of *Springer Series in Chemical Physics*, chap. 1, 3–23 (Springer, Berlin, Heidelberg, 2009), 1 edn.
- [10] Albright, T. A., Burdett, J. K. & Whangbo, M. *Orbital Interactions in Chemistry*, chap. 7, 134–136 (John Wiley & Sons, Inc., Hoboken, New Jersey, 2013), 2 edn.
- [11] Liu, Y., Wang, Y. & Bersuker, I. B. Geometry, electronic structure, and pseudo Jahn-Teller effect in tetrasilacyclobutadiene analogues. *Sci. Rep.* **6**, 23315 EP (2016).
- [12] Nakamura, K., Osamura, Y. & Iwata, S. Second-order Jahn-Teller effect of cyclobutadiene in low-lying states. An MCSCF study. *Chem. Phys.* **136**, 67 – 77 (1989).
- [13] Jusélius, J. & Sundholm, D. The aromaticity and antiaromaticity of dehydroannulenes. *Phys. Chem. Chem. Phys.* **3**, 2433–2437 (2001).
- [14] Karadakov, P. B. Aromaticity and antiaromaticity in the low-lying electronic states of cyclooctatetraene. *J. Phys. Chem. A* **112**, 12707–12713 (2008).
- [15] Hoffmann, R. *Solids and Surfaces: A Chemist's View of Bonding in Extended Structures* (Wiley-VCH, New York, 1989), 1 edn.
- [16] Hargittai, M., Réffy, B., Kolonits, M., Marsden, C. J. & Heully, J.-L. The structure of the free MnF₃ molecule — a beautiful example of the JahnTeller effect. *J. Am. Chem. Soc.* **119**, 9042–9048 (1997).
- [17] Sundholm, D., Berger, R. J. F. & Fliegl, H. Analysis of the magnetically induced current density of molecules consisting of annelated aromatic and antiaromatic hydrocarbon rings. *Phys. Chem. Chem. Phys.* **18**, 15934–15942 (2016).
- [18] Keith, T. A. & Bader, R. F. Calculation of magnetic response properties using a continuous set of gauge transformations. *Chem. Phys. Lett.* **210**, 223 – 231 (1993).
- [19] Bilde, M. & Hansen, A. E. Ab initio study of the Pauling-London-Pople (ring current) effect: LORG calculation and analysis of the NMR shielding tensors in a Sondheimer aromatic annulene and a non-aromatic analogue. *Mol. Phys.* **92**, 237–250 (1997).
- [20] Schmidt, M. W. *et al.* General atomic and molecular electronic structure system. *J. Comp. Chem.* **14**, 1347–1363.

- [21] Voter, A. F. & Goddard, W. A. The generalized resonating valence bond description of cyclobutadiene. *J. Am. Chem. Soc.* **108**, 2830–2837 (1986).
- [22] Schäfer, A., Horn, H. & Ahlrichs, R. Fully optimized contracted Gaussian basis sets for atoms Li to Kr. *J. Chem. Phys.* **97**, 2571–2577 (1992).
- [23] Allouche, A.-R. Gabedit – A graphical user interface for computational chemistry softwares. *J. Comp. Chem.* **32**, 174–182.
- [24] ReSpect 4.0.0 (2016), relativistic spectroscopy DFT program of authors M. Repisky, S. Komorovsky, V. G. Malkin, O. L. Malkina, M. Kaupp, K. Ruud, with contributions from R. Bast, R. Di Remigio, U. Ekstrom, M. Kadek, S. Knecht, L. Konecny, E. Malkin, I. Malkin Ondik (see <http://www.respectprogram.org>).
- [25] Dyall, K. G. Relativistic double-zeta, triple-zeta, and quadruple-zeta basis sets for the 4s, 5s, 6s, and 7s elements. *J. Phys. Chem. A* **113**, 12638–12644 (2009).
- [26] Persistence of Vision Pty. Ltd. (2004) Persistence of Vision Raytracer (Version 3.6) [Computer software], Retrieved from <http://www.povray.org/download/>.
- [27] Perdew, J. P., Ernzerhof, M. & Burke, K. Rationale for mixing exact exchange with density functional approximations. *J. Chem. Phys.* **105**, 9982–9985 (1996).

Acknowledgments

The work has been performed under the Project HPC-EUROPA3 (INFRAIA-2016-1-730897), with the support of the EC Research Innovation Action under the H2020 Programme; in particular, RB gratefully acknowledges the support of Prof. Dr. Dage Sundholm from the University of Helsinki and the computer resources and technical support provided by the CSC Helsinki. RB also acknowledges Prof. Dr. Dage Sundholm for financial support and Prof. Dr. Martin Breza from the Slovak University of Technology (Bratislava), Prof. Dr. Paolo Lazzeretti (Modena) and Prof. Dr. Juha Vaara (Oulu) for fruitful discussions and Prof. Dr. Nicola Hüsing (Salzburg) for generous and kind support of all research activities.

Author Contributions

RB provided the original idea performed the computational work and wrote the manuscript. AV provided the mathematical proof and the wrote the respective parts in the manuscripts.

Competing Interests

We declare that there were no competing interests.

Supplementary Information

The principle underlying antiaromaticity

Raphael J. F. Berger^{1*} and Alexandre Viel²

¹Department for Chemistry and Physics of Materials, University of Salzburg,
Jakob-Haringerstr 2a, A-5020 Salzburg, AUSTRIA

²8 Sente de la haie Saint-Marc, 78480 Verneuil sur Seine, FRANCE

*To whom correspondence should be addressed; E-mail: raphael.berger@sbg.ac.at.

S1 Group and representation theoretical details

While in mathematics a representation is “of” a group and “acting on a vector space”, placing the group first in order of importance, we instead talk in the main part this work of “representations of vector spaces” or “of operators”, “by a group”. This different phrasing is because the operators are what is more concrete in chemistry than the abstract groups.

A *point group* is a subgroup of $O(3)$, or from a more mathematical point of view, an abstract group together with a faithful representation of itself into $O(3)$. Thus two point groups can be isomorphic as abstract mathematical groups but be different representations at the same time (e.g. C_s and C_2), and for that be different point groups. The reason we want to separate the discussion of the group from the discussion of its representation is that we naturally encounter several representations by the same group.

The physical space \mathbb{R}^3 upon which the group elements act, serves as the representation space implied by the concept of a “point group”. Hence its axis (x, y, z) represent the algebraic generators of the physical quantities corresponding to operators or observables, which thereby can be analysed in terms of irreducible representations.

Once we have this representation ρ of physical space, we often want to describe its action on algebraically related spaces, such as direct sums, tensor spaces or dual spaces, or in the present case, angular-momentum space. Computing the representations of those more complex spaces from the initial representation of physical space can be described mathematically with the use of Schur functors. The functor that will interest us in order to describe the representation of the angular momentum operator is the second exterior power :

If we have a change of variable represented by an orthogonal linear map $\mathbf{r}' = U\mathbf{r}$, then $\nabla' = U\nabla$ because U is orthogonal, so that when transforming the angular momentum operator, we get $\mathbf{l}' = -i\hbar(\mathbf{r}' \times \nabla') = -i\hbar(U\mathbf{r} \times U\nabla) = (U \times U)\mathbf{l}$ where $U \times U$ (which can also be written $U \wedge U$, $[U \otimes U]$ or $Alt^2(U)$) is the application of the second exterior power to U . Finally since a representation is nothing but a family of orthogonal linear maps, we can also apply Schur functors to representations, so that if ρ is a representation of the physical space, $Alt^2(\rho)$ is the representation of the angular momentum operator.

Once we have identified this relationship, we gain the advantage of having computation rules, such as $Alt^2(\rho_1 \oplus \rho_2) = Alt^2(\rho_1) \oplus Alt^2(\rho_2) \oplus \rho_1 \otimes \rho_2$. The symmetric square functor Sym^2 is also of interest, it satisfies the same rule, and we have the functor decomposition $\rho \otimes \rho = Sym^2(\rho) \oplus Alt^2(\rho)$. Finally, if Γ is a real irreducible representation by a group G , then $Sym^2(\Gamma)$ always has exactly one totally symmetric Γ_0 component in its decomposition, so that for any two dimensional real irreducible representation E ,

$$E \otimes E = Alt^2(E) \oplus \Gamma_0 \oplus \rho_q; \quad dim(\Gamma_0) = 1, \quad dim(\rho_q) = 2. \quad (S1)$$

We also make a note that functors commute with restrictions. If F is a functor, ρ a representation by a group G , and H a subgroup of G , then for any $h \in H$, $F(\rho|_H)(h) = F(\rho|_H(h)) = F(\rho(h)) = (F(\rho))(h) = (F(\rho))|_H(h)$, so that $F(\rho|_H) = (F(\rho))|_H$. This works exactly the same way for bifunctors such as direct sums or tensor products of two representations.

We investigate what this entails when we look at the representation of the angular momentum operator of point groups. The main result we will want to prove is that the Alt^2 functor has a tendency to output the same (irreducible) representation when you give as input different irreducible representations of the same dimension.

All point groups can be partitioned into three families:

1. Point groups whose faithful representations decompose into three components, so that they embed in $O(1) \times O(1) \times O(1)$, *i.e.* groups that have no axis of rotation of order $n > 2$ (family \mathcal{K}_{aaa}). In detail $\mathcal{K}_{aaa} = \{C_1, C_i, C_2, C_s, C_{2v}, C_{2h}, D_2, D_{2h}\}$.
2. Point groups whose faithful representations decompose in two irreducible components but not three, so they embed in $O(1) \times O(2)$, *i.e.* groups that have a unique main axis of rotation of highest order n (family \mathcal{K}_{ae}). In detail $\mathcal{K}_{ae} = \{C_n, C_{nv}, C_{nh}, D_n, D_{nh}, D_{(n-1)d}, S_{2(n-1)}\}$, for $n > 2$
3. Point groups whose faithful representations are irreducible, *i.e.* groups that have more than one axis of rotation of order $n > 2$, which are also called isometric groups (family

\mathcal{K}_t). In detail $\mathcal{K}_t = \{T, T_d, T_h, O, O_h, I, I_h\}$.

It is not obvious that this partition defined in terms of a specific representation, carries down to the level of abstract groups independent of specific representations and we note that this is not true in general for abstract groups represented in $O(n)$ for $n > 3$.

Now we consider a point group from the first two families, whose representation is reducible, such that it decomposes into a direct sum $\rho = A \oplus E$.

An equivalent property is that the representation has a unique main symmetry axis, and then this axis is the subspace acted on by A : Let n be the maximum order of a rotation of the representation and consider the set of all the axis of the order n rotations. The group acts on this set of axis as the group acts by conjugation on the rotations : if a line l is the axis of a rotation $\rho(g)$ and $h \in G$, then $\rho(hgh^{-1})$ is a rotation whose axis is $\rho(h)(l)$. If there is only one such axis l (called the main symmetry axis), it means that $\rho(h)(l) = l$ for all $h \in G$, that is l is a subspace stabilized by G , so ρ is decomposes as a direct sum of the action on l and the action on its orthogonal. We will thus call this l (or A 's underlying vector space) the z -axis and its orthogonal (or E 's vector space) the (x, y) -plane.

In this \mathcal{K}_{ae} family, the angular momentum operator $Alt^2(\rho)$ decomposes into $Alt^2(\rho) = Alt^2(A) \oplus Alt^2(E) \oplus A \otimes E$. Since A is one dimensional, $Alt^2(A)$ is zero-dimensional and can be omitted : $Alt^2(\rho) = Alt^2(E) \oplus A \otimes E$.

Thus for point groups from \mathcal{K}_{ae} the (quantum mechanical) angular momentum (operator) decomposes into a one dimensional, hence irreducible, representation on the rotations around the z -axis $\Gamma_{\hat{l}_z} = Alt^2(E)$ (which is also the anti-symmetric square of the representation of the (x, y) -plane) and a two-dimensional representation $\Gamma_{\hat{l}_{x,y}} = A \otimes E$ on the rotations whose axis lie in the (x, y) -plane.

Moreover, $Sym^2(E)$ here further decomposes into $\Gamma_0 \oplus \rho_q$ where Γ_0 is the totally symmetric IR and ρ_q is some two-dimensional representation. In summary for groups from \mathcal{K}_{ae} we have:

$$E \otimes E = \underbrace{\Gamma_{\hat{l}_z}}_{=Alt^2(E)} \oplus \underbrace{\Gamma_0 \oplus \rho_q}_{=Sym^2(E)}; \quad \dim(\Gamma_0) = \dim(\Gamma_{\hat{l}_z}) = 1, \dim(\rho_q) = 2. \quad (S2)$$

We now want to prove the following property of their underlying abstract group, that given two (two-dimensional real irreducible) representations E_1, E_2 of point groups from \mathcal{K}_{ae} , then $Alt^2(E_1) = Alt^2(E_2)$, so that

$$\forall G \in \mathcal{K}_{ae}, \forall E \in Irrep(G, 2), Alt^2(E) = \Gamma_{\hat{l}_z} \quad (S3)$$

We start with finding out the possible underlying abstract groups from the families \mathcal{K}_{aaa} and \mathcal{K}_{ae} and show they belong to one of the four families $C_n, D_n, C_n \times C_2$ and $D_n \times C_2$. It is easy

to see that C_{nv} and D_n , C_{nh} and $C_n \times C_2$, D_{nh} and $D_n \times C_2$, D_{nd} and D_{2n} , and S_{2n} and C_{2n} are isomorphic. Then let G be a finite group faithfully represented in $O(1) \times O(2)$. This means we have two maps $\phi_i : G \rightarrow O(i)$ such that G is a subgroup of $G' = \phi_1(G) \times \phi_2(G)$. If ϕ_2 is not an isomorphism of G to $\phi_2(G)$, then $|G'| \geq |G| > |\phi_2(G)|$. But since $|G'|/|\phi_2(G)| = |\phi_1(G)|$ can only be 1 or 2, we must have $|\phi_1(G)| = 2$ and $|G'| = |G|$, so that $G = G'$. This proves that G is isomorphic to either a finite subgroup of $O(2)$, or to a product of one with C_2 .

We now prove the property for the finite subgroups C_n and D_n of $O(2)$. C_n are abelian groups, so their complex irreducible characters are all one-dimensional. Given a choice of generator of $g \in C_n$, for each n th root of unity ζ there is one character χ_ζ such that $\chi_\zeta(g) = \zeta$. The real irreducible representations are obtained by pairing χ_ζ with $\chi_{\bar{\zeta}}$ when ζ is not real and building their direct sum. Then, $\text{Alt}^2(\chi_\zeta \oplus \chi_{\bar{\zeta}}) = \chi_\zeta \otimes \chi_{\bar{\zeta}} = \chi_1 = 1$.

The dihedral groups D_n are generated by two elements r and s subject to the relations $r^n = s^2 = rsrs = e$. They have complex two-dimensional irreducible representations ρ_k , given by the assignments

$$r \mapsto \begin{pmatrix} \cos \frac{2k\pi}{n} & -\sin \frac{2k\pi}{n} \\ \sin \frac{2k\pi}{n} & \cos \frac{2k\pi}{n} \end{pmatrix}, \text{ and } s \mapsto \begin{pmatrix} 1 & 0 \\ 0 & -1 \end{pmatrix}, \text{ for } 0 < k < n/2.$$

Then $\text{Alt}^2(\rho_k)(r) = (1)$ and $\text{Alt}^2(\rho_k)(s) = (-1)$, which are independent of k .

This proves the claim for the C_n and D_n families. As for the $C_n \times C_2$ and $D_n \times C_2$ families, their irreducible representations are tensor products of one irreducible representation of each. Since we are in dimension 2, for any E representation of C_n or D_n and A representation of C_2 , we have $\text{Alt}^2(E \otimes A) = \text{Alt}^2(E) \otimes (A \otimes A) = \text{Alt}^2(E) \otimes \Gamma_0$, which is independent of the choice E and A .

The determination of the irreducible representations of these groups shows that our classification of point groups is also a classification at the level of abstract groups: we have shown in all cases that there was no three-dimensional irreducible representation of G . So in particular the families \mathcal{K}_{aaa} and \mathcal{K}_{ae} of groups are disjoint from the family \mathcal{K}_t .

Moreover, if $n \geq 3$ then G cannot be faithfully represented by a direct sum of three one dimensional representations as then G cannot have any element of order higher than two. Thus any faithful representation of these groups in $O(3)$ has an $A \oplus E$ shape and has a unique main axis of symmetry. These groups form the family \mathcal{K}_{ae} .

Finally, if $n \leq 2$ then there are no two-dimensional irreducible representations of G , so these groups form the \mathcal{K}_{aaa} family. In their case, the choice of a z -axis needs more than just algebraic considerations.

Consider now a point group from the family \mathcal{K}_t , *i.e.* an isometric point group, it comes with a faithful irreducible representation T into $O(3)$. Such a point group cannot distinguish between

the three coordinate axis x, y and z . Then the angular momentum representation $\Gamma_{\hat{t}} = \text{Alt}^2(T)$ is irreducible. For three-dimensional representations, $\text{Alt}^2(\text{Alt}^2(T)) = \det(T) \otimes T$, so if $\text{Alt}^2(T)$ was reducible, the reducibility would carry over to $\det(T) \otimes T$, and then by tensoring again with $\det(T)$, to T itself.

Among the cubic point groups, this is a subfamily of the isometric point groups consisting of T, T_d, T_h, O and O_h , a similar property is true: if T_1 and T_2 are two irreducible three-dimensional representations, then $\text{Alt}^2(T_1) = \text{Alt}^2(T_2) = \Gamma_{\hat{t}}$. This is because in every case, there is a one dimensional representation A such that $T_2 = A \otimes T_1$, so that $\text{Alt}^2(T_2) = \text{Alt}^2(T_1) \otimes A \otimes A = \text{Alt}^2(T_1)$. Among the icosahedral groups (I, I_h), this is no longer true. Here also the symmetric square $\text{Sym}^2(T)$ further decomposes into $\Gamma_0 \oplus \rho_q$ where ρ_q is some five-dimensional representation.

S2 Computational details

S2.1 C_4H_4

The geometry optimization of 1,3-cyclobutadiene in D_{4h} symmetry was performed with the GAMESS-US^{S20} programme package (version 5DEC 2014 (R1)) for a reason lined out below and in the spirit of an early work from Voter and Goddard at the generalized valence bond - perfect pairing (GVB(PP)) level of theory^{S21} and using the Karlsruhe def-TZVPP basis sets for carbon and hydrogen^{S22}. Starting orbitals and geometry were used from a restricted Hartree-Fock (RHF) calculation for the dianionic species $[\text{C}_4\text{H}_4]^{2-}$, restricted to D_{4h} spatial symmetry (but the wave function is effectively treated in GAMESS as D_{2h} since no higher wave function symmetries are available in the current versions of GAMESS-US). For the sub-sequential GVB run 13 doubly occupied inactive orbitals and 1 electron pair in 2 orbitals were set. That setting completely is equivalent to a complete active space two electrons in two orbitals computation (CAS(2i2)). We note that convergence of GVB in cases can be considerably slower and in cases of problems with the starting orbitals it seems convenient to converge the orbitals in an actual CAS(2i2) run, that for example can be run using the full-Newton-Raphson converger that is implemented in GAMESS-US. The main reason for choosing GVB(PP) instead of CAS was to be able to extract orbital energies from a “multiconfigurational” wave function, in order to demonstrate the branching and energy changes of the orbitals, that is essential for the *primoid* second order Jahn-Teller cases.

The optimization resulted in the following structure and energy:

C4H4.D4h.eq.GVB-PP.TZVPP.txt

C4H4, D4h, GVB(PP)/def-TZVPP, units of and hartree

E= -153.6925014955 GRAD. MAX= 0.0000280 R.M.S.= 0.0000162

C	6.0	-0.7131801506	-0.7131801826	-0.0000000000
C	6.0	0.7131801506	-0.7131801826	0.0000000000
C	6.0	-0.7131801506	0.7131801826	0.0000000000
C	6.0	0.7131801506	0.7131801826	0.0000000000
H	1.0	-1.4687380037	-1.4687382006	-0.0000000000
H	1.0	1.4687380037	-1.4687382006	0.0000000000
H	1.0	-1.4687380037	1.4687382006	0.0000000000
H	1.0	1.4687380037	1.4687382006	0.0000000000

The D_{2h} minimum was calculated by choosing D_{2h} symmetry in the input and slightly distorting the coordinates to some off- x, y -diagonal value but using the starting orbitals from the D_{4h} run. The optimization resulted in the following structure and energy:

C4H4.D2h.eq.GVB-PP-TZVPP.txt

C4H4, D2h, GVB(PP)/def-TZVPP, units of and hartree

E= -153.7126953359 GRAD. MAX= 0.0000191 R.M.S.= 0.0000099

C	6.0	-0.7761786150	-0.6619033512	0.0000000000
C	6.0	0.7761786150	-0.6619033512	-0.0000000000
C	6.0	-0.7761786150	0.6619033512	-0.0000000000
C	6.0	0.7761786150	0.6619033512	-0.0000000000
H	1.0	-1.5315443480	-1.4196296797	0.0000000000
H	1.0	1.5315443480	-1.4196296797	-0.0000000000
H	1.0	-1.5315443480	1.4196296797	-0.0000000000
H	1.0	1.5315443480	1.4196296797	-0.0000000000

By a linear interpolation between the D_{4h} saddle point and the D_{2h} minimum structure 9 intermediate structures were generated and the frontier orbital energies were extracted to generate a branching plot (see Fig. S2), a schematic version of which is represented in Fig. 1 in the main text.

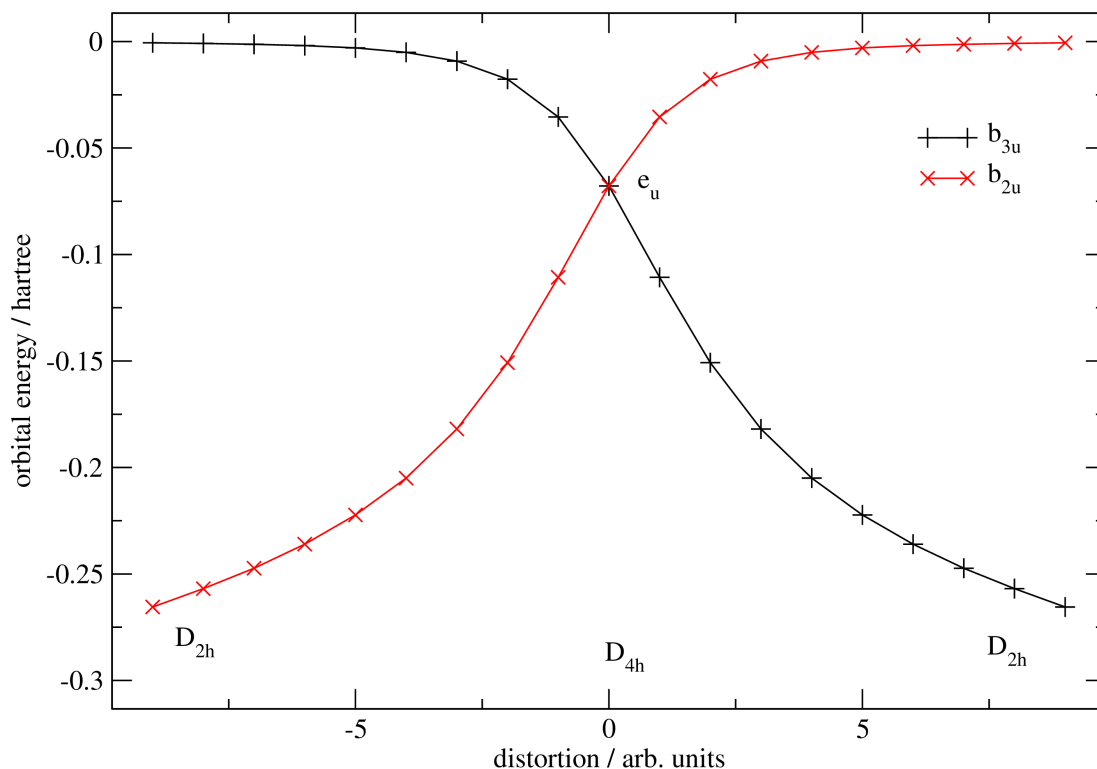


Figure S1: Frontier orbital branching in C_4H_4 upon relaxed distortion from D_{4h} to D_{2h} at GVB(PP)/def-TZVPP level of theory.

The corresponding state energies of first two singlet states (1^1A_g and 2^1A_g) have been computed for the intermediate structures complemented by two more strongly distorted structures by the analogous CAS(2i2) state average calculation. In this way one can see a representation of the JT-coupling between the two states (see Fig. S1).

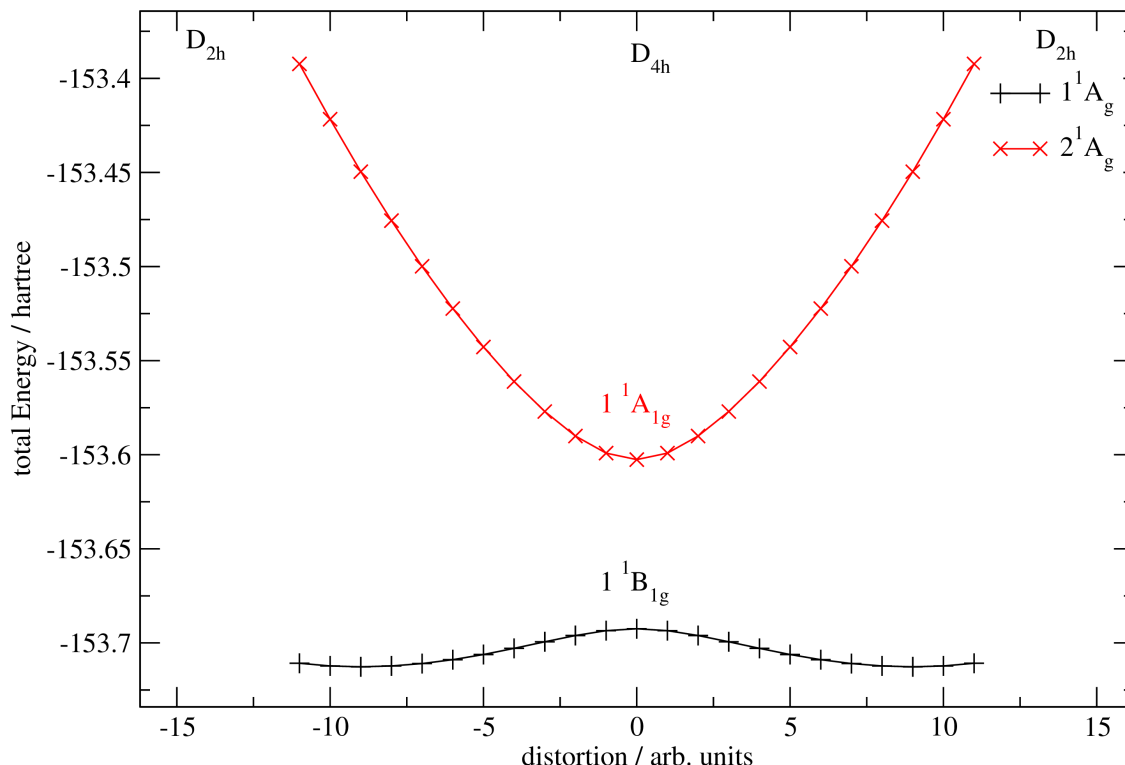


Figure S2: Lowest two singlet states of C_4H_4 (1^1B_{1g} and 1^1A_{1g}) in D_{4h} symmetry. Upon distortion to D_{2h} they restrict to 1^1A_g and 2^1A_g , respectively. Energies taken from GVB(PP)/def-TZVPP level of theory. The elevation to a (local) maximum at $x = 0$ in the ground state level, can be interpreted as an effect of a second order Jahn-Teller coupling between the two levels by the distortional mode, which is represented by B_{1g} .

The orbital plots in Figures 2, 5 and 7 were generated with the program gabedit^{S23}.

Magnetically induced currents were calculated for the D_{2h} minimum structure using the program ReSpect (version 4.0.0) from Repisky and Komorovsky^{S24}. Since for the D_{2h} minimum structure the CI coefficients of the two configurations from the GVB(PP) calculation were only 0.980137, and -0.198321 respectively (corresponding to a weight of only about 4% of the second configuration), a single reference method can be used safely for computation of the magnetic response. To stay consistent we have also used for the magnetic response the HF level of theory and the Dyalls (relativistic) triple- ζ basis sets for C and H^{S25}.

For the wave function calculation the GVB(PP) structure has been used a point nucleus

model, the “mdhf” method (multicomponent Dirac-HF hamiltonian) but quasi-non relativistic settings “cscale=20.0” and “soscale=0.0” and “grid: large”.

The magnetic response calculation was done using the London orbital approach (GIAO) and the ‘ ‘dft-kernel: xalda” option and the magnetic field was set perpendicular to the molecular plane.

The integration grid for the total current calculation was set to start -4 Å below the molecular plane pass the centre of the molecule and have a width and heights of 8 Å, respectively and using 200×200 grid points. The net currents passing that plane are calculated to 2.6748885 nA/T (diatropic) and -25.132882 nA/T (paratropic) yielding a total paratropic current of -22.457993 nA/T.

The streamline plot from Fig. 3 were generated similarly just using a current plane starting at $x = -2.5$ and $y = -2.5$ Å. The length and width was set to 5 Å. The streamline plot was generated using the “make-stream” script that is distributed with ReSpect. Fig. 3 was generated with Povray^{S26}.

S2.2 C₈H₈

Similar as C₄H₄ also C₈H₈ in full D_{8h} symmetry is a multi-reference case of two electrons in the doubly degenerate e_{2u} orbitals^{S14}, that has to be treated at least with a two-configuration wave function. For consistency we have applied here as well the GVB(PP)/TZVPP method with completely analogous strategy as in the case of C₄H₄, that is first optimization of the dianion using RHF and then followed by the symmetry restricted geometry optimization in D_{8h} with GVB using 27 doubly occupied orbitals and two orbitals with two electrons in perfect pairing to yield a second order saddle point structure (with two equally weighted configurations):

C8H8.D8h_eq_GVB-PP_TZVPP.txt

C8H8, D8h, GVB(PP)/def-TZVPP, units of and hartree

E=-307.5867677504

C	1.6802926394	0.0000000000	0.6960000000
C	-1.6802926394	0.0000000000	0.6960000000
C	1.6802926394	0.0000000000	-0.6960000000
C	-1.6802926394	0.0000000000	-0.6960000000
C	-0.6960000000	0.0000000000	-1.6802926394
C	0.6960000000	0.0000000000	1.6802926394
C	-0.6960000000	0.0000000000	1.6802926394
C	0.6960000000	0.0000000000	-1.6802926394
H	2.6743870164	0.0000000000	1.1077673732
H	-2.6743870164	0.0000000000	1.1077673732
H	2.6743870164	0.0000000000	-1.1077673732
H	-2.6743870164	0.0000000000	-1.1077673732
H	1.1077673732	0.0000000000	2.6743870164

H	-1.1077673732	0.0000000000	2.6743870164
H	1.1077673732	0.0000000000	-2.6743870164
H	-1.1077673732	0.0000000000	-2.6743870164

The C-C distance is 1.392 and H-H is 1.076 Å, respectively, the energy of the HOMO $\varepsilon(e_{2u}) = -0.0608$ Hartree.

Subsequent optimization in D_{4h} results in a first order saddle point, with already a small coefficient of the second configuration ($c_1 = 0.995999$, $c_2 = -0.089369$) and HOMO and LUMO energies of $\varepsilon(b_{3u}) = -0.2699$ and $\varepsilon(b_{2u}) = 0.0000$ Hartree, the C-C distances split into two sets of 1.324 and 1.473 Å and C-H distances of 1.075 Å:

C8H8_D4h_eq_GVB-PP_TZVPP.txt

C8H8, D4h, GVB(PP)/def-TZVPP, units of and hartree

E=-307.6196129777

C	1.6689419240	-0.0000000000	0.7365511863
C	1.6689419240	-0.0000000000	-0.7365511863
C	-1.6689419240	-0.0000000000	0.7365511863
C	-1.6689419240	-0.0000000000	-0.7365511863
C	0.7382750555	0.0000000000	1.6782476200
C	0.7382750555	0.0000000000	-1.6782476200
C	-0.7382750555	0.0000000000	1.6782476200
C	-0.7382750555	0.0000000000	-1.6782476200
H	2.6649503331	0.0000000000	1.1423860279
H	2.6649503331	0.0000000000	-1.1423860279
H	-2.6649503331	0.0000000000	1.1423860279
H	-2.6649503331	0.0000000000	-1.1423860279
H	1.1298611754	0.0000000000	2.6795220078
H	1.1298611754	0.0000000000	-2.6795220078
H	-1.1298611754	0.0000000000	2.6795220078
H	-1.1298611754	0.0000000000	-2.6795220078

Releasing the symmetry to D_{2d} yields the minimum structure, with again smaller CI coefficient for the second configuration ($c_1 = 0.999143$, $c_2 = -0.041393$) and HOMO and LUMO energies of $\varepsilon(a_1) = -0.3578$ and $\varepsilon(a_2) = 0.0000$ Hartree; geometric parameters are $C-C_{short/long} = 1.320/1.475 \text{ \AA}$, $C-H = 1.077 \text{ \AA}$, $\angle(CCC) = 127.3^\circ$, $\angle^{dih}(CCCC) = 0.0/54.1^\circ$.

C8H8_D2d_eq.GVB-PP_TZVPP.txt

C8H8, D2d, GVB(PP)/def-TZVPP, units of and hartree

E=-307.6408330022

C	-1.5659424	0.6328078	0.3790173
C	1.5659424	0.6328078	-0.3790173
C	-1.5659424	-0.6328078	-0.3790173
C	1.5659424	-0.6328078	0.3790173
C	-0.6328078	1.5659424	0.3790173
C	0.6328078	-1.5659424	0.3790173
C	-0.6328078	-1.5659424	-0.3790173
C	0.6328078	1.5659424	-0.3790173
H	-2.4628900	0.8232252	0.9441068
H	2.4628900	-0.8232252	0.9441068
H	-2.4628900	-0.8232252	-0.9441068
H	2.4628900	0.8232252	-0.9441068
H	0.8232252	-2.4628900	0.9441068
H	-0.8232252	2.4628900	0.9441068
H	0.8232252	2.4628900	-0.9441068
H	-0.8232252	-2.4628900	-0.9441068

The magnetically induced currents for the D_{2d} minimum structure were calculated with the very same procedures as in case of C_4H_4 and the magnetic field was set perpendicular to the average molecular plane. The integration grid for the total current calculation was set to start -5 \AA below the molecular plane pass the centre of the molecule and have a width and heights of 10 \AA , respectively 300×300 grid points. The net currents passing that plane are calculated to 5.7644395 nA/T (diatropic) and -8.2361711 nA/T (paratropic) yielding a total paratropic current of -2.4717316 nA/T . The streamline plot from Fig. 3 were generated similarly just using a current plane starting at $x = 6$ and $y = -6 \text{ \AA}$. The length and width was set to 12 \AA .

S2.3 MnF₃

For the calculation of the magnetically induced molecular currents in MnF₃, we have used the experimental gas-phase structure, that is C_{2v} symmetric and corresponds to the minimum of the 5B_1 electronic state^{S16} (Mn-F1= 1.728Å, Mn-F2= 1.754Å, Mn-F3= 1.754Å and $\angle(\text{F2-Mn-F3})= 143.3^\circ$). We have used the PBE0 hybrid density functional^{S27} as it is implemented in ReSpect (“method : mdks/pbe0”), the non-relativistic settings as described above, “multiplicity : 5” and again the relativistic basis sets from Dyall for Mn and F atoms^{S25}. In the magnetic response calculation the DFT kernel option “xalda” was chosen. The grid plane for the current vectors was set to the $z = 0$ plane extending 8 Å in x and y direction respectively with a grid of 50×50 points. Otherwise the same procedure was applied as in case of C₄H₄ and C₈H₈.

S3 On the physical and chemical interpretation and connection of induced paramagnetism and bonds

Yet a more generalizing way of view is that diamagnetism indicates situations of electron delocalized bonds while paramagnetism indicates situations of incompletely filled molecular shells. And adopting a purely physical point of view, one can formulate, that proper bonds have a tendency to undergo precession motions in the same way electrons would that are orbiting in quasi-classically stable trajectories, while for symmetry reasons instable trajectories from a near-degenerate trajectory space lead to precession motions within this space but in opposite direction as compared to the diamagnetic case.

The symmetry connection between rotational virtual excitations and the Jahn-Teller effect in a subfamily of the point groups deepens our understanding of antiaromaticity. On the one hand, this connection, however cannot be established in the general case of an antiaromatic molecule by pure symmetry considerations, not even in the case of a relatively high symmetry like pentalene. This is the usual restriction underlying any symmetry selection rule (take dipole transitions for electronic excitations by light). An open question in this context also is if there is a deeper connection between the numerator and the denominator in expression 3, which intuition might suggest: two orbitals that are very similar in shape and only differ by orientation necessarily should have similar energies. An open question is: In how far can we expect the opposite as well?

On the other hand the bare symmetry rule or numerical principle (*i.e.* the conditions under which to observe large terms 3) again cannot provide us with a precise condition as to when a specific case is to be considered antiaromatic and when not. We even notice a paradoxical component: the stronger the distortion the smaller the terms in expression 3 are getting (by both an increase in the denominator and a decrease in the numerator) and the weaker the paramagnetic response will be in general. Also a strong paramagnetic response shall make one expect a low degree of distortion as well. In that sense we rather expect that all systems that meet the IUPAC

definition (that without a doubt by construction is based on observed real world examples) are those that find a kind of balance between the extremes of distortion and paramagnetism. C_8H_8 misses it due to the strong distortion while there might be other cases of strong paramagnetism that show less or no distortion contrary to expectation. Take for example a transition state of a $2 + 2$ cycloaddition reaction.

Thus the concept of antiaromaticity appears as a principle of instability. Nevertheless it is a concept that can be sensitively verified (or falsified) both in the real world and in the computer by energetic, structural and magnetic methods.

S4 IUPAC definition of Antiaromaticity

The definition of antiaromaticity which made it into the IUPACs “Gold-Book” was originally provided by V. I. Mishkin in his article about “Glossary of terms used in theoretical organic chemistry”^{S5}. The complete quote is “antiaromaticity (antithetical to aromaticity)

Those cyclic molecules for which cyclic electron delocalization provides for the reduction (in some cases, loss) of thermodynamic stability compared to acyclic structural analogues are classified as antiaromatic species. In contrast to aromatic compounds, antiaromatic ones are prone to reactions causing changes in their structural type, and display tendency to alternation of bond lengths and fluxional behavior (see fluxional molecules) both in solution and in the solid. Antiaromatic molecules possess negative (or very low positive) values of resonance energy and a small energy gap between their highest occupied and lowest unoccupied molecular orbitals. In antiaromatic molecules, an external magnetic field induces a paramagnetic electron current. Whereas benzene represents the prototypical aromatic compound, cyclobuta-1,3-diene exemplifies the compound with most clearly defined antiaromatic properties.”

References

- [S1] Solà, M. Connecting and combining rules of aromaticity. Towards a unified theory of aromaticity. *WIREs, Comp. Mol. Sci.* (2018).
- [S2] Janda, T. & Foroutan-Nejad, C. Why is benzene unique? Screening magnetic properties of C_6H_6 isomers. *Chem. Phys. Chem.* **19**, 2357–2363 (2018).
- [S3] Breslow, R. Antiaromaticity. *Acc. Chem. Res.* **6**, 393–398 (1973).
- [S4] International Union of Pure and Applied Chemistry, IUPAC Compendium of Chemical Terminology – The Gold Book (2006).

- [S5] Minkin, V. I. Glossary of terms used in theoretical organic chemistry — Pure and Applied Chemistry. *Pure Appl. Chem.* **71**, 1919 – 1981 (2009).
- [S6] Lazzeretti, P. Ring currents. *Prog. Nuc. Mag. Res. Spec.* **36**, 1 – 88 (2000).
- [S7] Steiner, E. & Fowler, P. W. Four- and two-electron rules for diatropic and paratropic ring currents in monocyclic systems. *Chem. Commun.* 2220–2221 (2001).
- [S8] Sulzer, D., Olejniczak, M., Bast, R. & Saue, T. 4-component relativistic magnetically induced current density using London atomic orbitals. *Phys. Chem. Chem. Phys.* **13**, 20682–20689 (2011).
- [S9] Bersuker, I. B. Recent developments in the Jahn–Teller effect theory. In Köppel, H., Yarkony, D. & Barentzen, H. (eds.) *The Jahn-Teller Effect*, vol. 97 of *Springer Series in Chemical Physics*, chap. 1, 3–23 (Springer, Berlin, Heidelberg, 2009), 1 edn.
- [S10] Albright, T. A., Burdett, J. K. & Whangbo, M. *Orbital Interactions in Chemistry*, chap. 7, 134–136 (John Wiley & Sons, Inc., Hoboken, New Jersey, 2013), 2 edn.
- [S11] Liu, Y., Wang, Y. & Bersuker, I. B. Geometry, electronic structure, and pseudo Jahn-Teller effect in tetrasilacyclobutadiene analogues. *Sci. Rep.* **6**, 23315 EP (2016).
- [S12] Nakamura, K., Osamura, Y. & Iwata, S. Second-order Jahn-Teller effect of cyclobutadiene in low-lying states. An MCSCF study. *Chem. Phys.* **136**, 67 – 77 (1989).
- [S13] Jusélius, J. & Sundholm, D. The aromaticity and antiaromaticity of dehydroannulenes. *Phys. Chem. Chem. Phys.* **3**, 2433–2437 (2001).
- [S14] Karadakov, P. B. Aromaticity and antiaromaticity in the low-lying electronic states of cyclooctatetraene. *J. Phys. Chem. A* **112**, 12707–12713 (2008).
- [S15] Hoffmann, R. *Solids and Surfaces: A Chemist's View of Bonding in Extended Structures* (Wiley-VCH, New York, 1989), 1 edn.
- [S16] Hargittai, M., Réffy, B., Kolonits, M., Marsden, C. J. & Heully, J.-L. The structure of the free MnF_3 molecule — a beautiful example of the JahnTeller effect. *J. Am. Chem. Soc.* **119**, 9042–9048 (1997).
- [S17] Sundholm, D., Berger, R. J. F. & Fliegl, H. Analysis of the magnetically induced current density of molecules consisting of annelated aromatic and antiaromatic hydrocarbon rings. *Phys. Chem. Chem. Phys.* **18**, 15934–15942 (2016).
- [S18] Keith, T. A. & Bader, R. F. Calculation of magnetic response properties using a continuous set of gauge transformations. *Chem. Phys. Lett.* **210**, 223 – 231 (1993).

- [S19] Bilde, M. & Hansen, A. E. Ab initio study of the Pauling-London-Pople (ring current) effect: LORG calculation and analysis of the NMR shielding tensors in a Sondheimer aromatic annulene and a non-aromatic analogue. *Mol. Phys.* **92**, 237–250 (1997).
- [S20] Schmidt, M. W. *et al.* General atomic and molecular electronic structure system. *J. Comp. Chem.* **14**, 1347–1363.
- [S21] Voter, A. F. & Goddard, W. A. The generalized resonating valence bond description of cyclobutadiene. *J. Am. Chem. Soc.* **108**, 2830–2837 (1986).
- [S22] Schäfer, A., Horn, H. & Ahlrichs, R. Fully optimized contracted Gaussian basis sets for atoms Li to Kr. *J. Chem. Phys.* **97**, 2571–2577 (1992).
- [S23] Allouche, A.-R. Gabedit – A graphical user interface for computational chemistry softwares. *J. Comp. Chem.* **32**, 174–182.
- [S24] ReSpect 4.0.0 (2016), relativistic spectroscopy DFT program of authors M. Repisky, S. Komorovsky, V. G. Malkin, O. L. Malkina, M. Kaupp, K. Ruud, with contributions from R. Bast, R. Di Remigio, U. Ekstrom, M. Kadek, S. Knecht, L. Konecny, E. Malkin, I. Malkin Ondik (see <http://www.respectprogram.org>).
- [S25] Dyall, K. G. Relativistic double-zeta, triple-zeta, and quadruple-zeta basis sets for the 4s, 5s, 6s, and 7s elements. *J. Phys. Chem. A* **113**, 12638–12644 (2009).
- [S26] Persistence of Vision Pty. Ltd. (2004) Persistence of Vision Raytracer (Version 3.6) [Computer software], Retrieved from <http://www.povray.org/download/>.
- [S27] Perdew, J. P., Ernzerhof, M. & Burke, K. Rationale for mixing exact exchange with density functional approximations. *J. Chem. Phys.* **105**, 9982–9985 (1996).